Journal of Materials Chemistry B

ROYAL SOCIETY OF CHEMISTRY

PAPER

View Article Online
View Journal

Cite this: DOI: 10.1039/d6tb00534a

Wearable near-infrared LED photothermal microneedle patch reduces periorbital wrinkles in a randomized pilot clinical trial

Hyo-Won Han,†[a] Dong-Hwan Lee,†[b] Ara Joe,[a] Yeong Jun Jeon,[c] Yu-Ra Lim,[c] Sang Bong Lee,[d] Bum-Ho Bin,[b] JuKyung Lee,[e] Thavasyappan Thambi,[f] João Conde,*[g] Panchanathan Manivasagan*[c] and Eue-Soon Jang*[ac]

Microneedle patches are typically passive, limiting control over dissolution kinetics and transdermal transport. Here we introduce a wearable, actively actuated microneedle system in which dissolving hyaluronic-acid tips penetrate the stratum corneum while a hydrocolloid backing embedded with hyaluronic-acid–gold-nanorod (HA–GNR) nanocomposites provides near-infrared (NIR, ≈780 nm) photothermal actuation. Under brief LED illumination, the GNRs deliver a mild, eyelid-safe thermal micro-dose (∼41 °C) that accelerates tip dissolution and enhances short-range transport without increasing needle length. Tissue-mimicking phantoms show heat-augmented dye advance (≈5.1 mm *vs.* ≈2.6 mm at 15 min), supporting a mechanism involving accelerated dissolution and enhanced localized transport driven by combined diffusion and micro-convective effects. In a monocentric, randomized, investigator-blinded pilot trial (n = 20 women, 30–59 year) with thrice-weekly use for four weeks, under-eye PRIMOS average roughness (R_a) improved by 16.3% at week 4 ($p < 0.001$), and periorbital brightness (VISIA-CR L^*) increased by ∼1.5–2.0%. A with-/without-NIR comparison at the crow's-feet favored actuation (∼14.1% *vs.* ∼1.9% improvement at week 4). No device-related adverse events were observed. By decoupling penetration from actuation through a plasmonic nanocomposite backing, this platform transforms dissolving microneedles into programmable, eyelid-compatible transdermal devices with human evidence, suggesting broad utility for gentle, controllable delivery at sensitive sites.

Received 9th March 2026,
Accepted 2nd May 2026

DOI: 10.1039/d6tb00534a

rsc.li/materials-b

1. Introduction

Skin aging is a prominent indicator of physical age,[1] with periorbital skin being the most susceptible given that it is the thinnest part of the face.[2] The eye is the most sensitive and fragile region of the skin.[3] Aging, lack of sleep, daily stress, radiation, smoking, and environmental pollutants contribute to the development of crow's feet and periorbital wrinkles, resulting in a tired appearance.[4–6] Filler injections are low-cost cosmetic treatments that involve the injection of a gel-like material under the skin to improve wrinkles or soft tissues.[7] However, intravascular filler injections can have serious side effects, including skin necrosis, visual loss, and facial over-filling syndrome.[8–11] The increasing demand for aesthetic medical procedures has recently sparked public interest in specialist consultations with dermatologists, resulting in an urgent need to develop an efficient, safe, and innovative at-home eye-wrinkle cosmetic product to satisfy customer demands and improve the quality of life.[12] Microneedle patches have emerged as a popular at-home anti-wrinkle product among the many anti-wrinkle cosmetic products available on the market (*e.g.*, creams, lotions, facial masks, moisturizers, and fabrics).[13–16]

Recently, microneedle patch technology has been increasingly used in the field of aesthetic medicine, given its

[a] *Golden Crow Co., Ltd., Global building #140, Daehak-ro 61, Gumi, Gyeongbuk 39177, Republic of Korea. E-mail: euesoon@kumoh.ac.kr*
[b] *Department of Applied Biology, Ajou University, Kyonggi-do, Republic of Korea, and 206, Worldcup-ro, Yeongtong-gu, Suwon-si, Gyeonggi-do, 16499, Republic of Korea*
[c] *Department of Chemistry and Bio Science, Kumoh National Institute of Technology, Daehak-ro 61, Gumi, Gyeongbuk 39177, Republic of Korea. E-mail: manimaribtech@gmail.com*
[d] *Department of Nursing, Chung Cheong University, Cheongju, Chungbuk, Republic of Korea*
[e] *Digital Health Care Research Center, Gumi Electronics and Information Technology Research Institute (GERI), Gumi, Gyeongbuk 39253, Republic of Korea*
[f] *Graduate School of Biotechnology, College of Life Sciences, Kyung Hee University, Yongin-si, Gyeonggi-do 17104, Republic of Korea*
[g] *Comprehensive Health Research Centre (CHRC), NOVA Medical School, Faculdade de Ciências Médicas, NMS/FCM, Universidade NOVA de Lisboa, Lisboa, Portugal. E-mail: joao.conde@nms.unl.pt*
† These authors contributed equally.

advantages, such as painlessness, high safety, and ease of use. Furthermore, given the length and thickness of the needles, it can be used as a non-invasive home skin care device for treating wrinkles.[2] Microneedles are extremely small, submillimeter-sized needles arranged in an array to penetrate the outer skin layer.[17–20] Recently, a photothermal microneedle patch (PMP) that combines microneedle technology with photothermal therapy (PTT) has emerged as an innovative approach to improve periorbital wrinkles.[21] PMPs are composed of polymers and photothermal (PT) agents, including hyaluronic acid (HA) and gold nanorods (GNRs). HA is a naturally occurring biopolymer consisting of repeating disaccharide units of D-glucuronic acid and *N*-acetyl-D-glucosamine, which are endogenous components of human skin and the extracellular matrix of human tissues.[22] HA is a versatile material with several unique properties, including water-binding capacity, swelling, biocompatibility, biodegradability, and safety, making it a suitable candidate for developing safe cosmetic products aimed at improving wrinkles, moisture, and elasticity in dermatology.[23,24]

PTT has emerged as an effective therapeutic approach for treating cancer and microbial infections because of its non-invasiveness, ease of operation, high spatiotemporal resolution, high specificity, and low side effects.[25] PT materials are used to convert NIR light into heat energy (>43 °C) when exposed to external NIR light sources.[26] PT materials, such as GNRs, are most commonly used in PTT because of their unique properties, such as excellent biocompatibility, high PT conversion efficiency, easy synthesis, and high absorption in the NIR region, resulting in a better enhancement of PT heat generation to improve wrinkle appearance, create smoother skin, and achieve a more youthful appearance.[27] In recent years, PT microneedle systems have advanced rapidly for controlled drug administration, wound healing, and minimally invasive therapeutic applications have advanced rapidly in recent years, particularly through NIR-responsive platforms that allow fine spatiotemporal management of treatment effects.[28–31] However, photothermal agents are directly integrated into the microneedle matrix in most described systems, which may lead to uneven heat distribution and greater skin exposure to nanomaterials. Despite these developments, few studies have focused on the creation of safe, regulated, and user-friendly at-home PT microneedle systems, and their application in delicate cosmetic areas, such as the periorbital area, remains largely underexplored.[32,33]

In this study, we developed the first PT-responsive soluble microneedle patch (PMP) as a novel emerging at-home cosmetic product for improving periorbital wrinkles (Scheme 1). The developed PMP comprises cross-linked HA particulate-based needle tips and an HA-GNR-based hydrocolloid pad as the back surface. Notably, HA-based microneedle tips and the top of the thin film of the adhesive hydrocolloid pad were in direct contact with the skin, which did not have GNRs, and demonstrated that HA-GNRs were successfully fabricated on the back of the hydrocolloid pad. The fabricated PMP was applied horizontally under the eyes and vertically in the crow's feet region, and it was gently pressed for 5 s to reach the upper epidermis without pain, bleeding, redness, injury, or infection. A NIR light-emitting diode (LED) eye mask device (780 nm), worn over microneedle patches, ensures a safe temperature increase (41.0 °C) for eyelid warming; this reduces wrinkles, fine lines, and other signs of aging, while improving skin rejuvenation, tightening, elasticity, texture, collagen production, fibroblast activation, and dermal blood flow. Our results confirm that PMP with NIR LED light is a new, safe, and effective home-use cosmetic product for improving periorbital wrinkles and can become a highly valuable cosmetic product that can improve the quality of life in the future.

2. Materials and methods

2.1. Materials

Benzyldimethylhexadecylammonium chloride (BDAC), gold(III) chloride trihydrate ($HAuCl_4 \cdot 3H_2O$), sodium borohydride ($NaBH_4$), hexadecyltrimethylammonium bromide (CTAB), L-ascorbic acid, silver nitrate ($AgNO_3$), agarose, methylene blue, sodium hydroxide (NaOH), and 1,4-butanediol diglycidyl ether (BDDE) were supplied by Sigma-Aldrich (USA). Hyaluronic acid (HA) was obtained from SK Bioland Co., Ltd. (Cheonan, Korea). Hibitane solution was supplied by Tokyo Kasei Kogyo Co., Ltd. (Tokyo, Japan). Ultrapure water was produced using an aquaMAX-Ultra 370 water purification system (YL Instrument Co., Ltd, Korea) and used in all experiments.

2.2. Clinical study design and participants

This prospective study was a monocentric, randomized, investigator-blinded, controlled pilot trial for investigating the efficiency and safety of a PMP system to treat periorbital wrinkles and crow's feet. This study was reviewed and approved by the Cutis Institutional Review Board of the Human Research Ethics Committee of the Cutis Biomedical Research Center (Seoul, Korea). All volunteers provided written informed consent and agreed to produce digital photographs before the study (Approval number: CBRC-E-211115-58). The volunteers were selected based on their ability to be monitored and followed during experiments. A total of 20 healthy Korean women aged 30–59 years were enrolled in this pilot study conducted between November 2021 and January 2022. All participants had mild-to-moderate periorbital wrinkles according to the wrinkles scale and sought aesthetic improvements in the facial region.[34] None of the participants had dermatologic diseases, were pregnant, or breastfed.

2.3. Photothermal microneedle patch (PMP)

The cross-linked HA particulate and PMP were designed and developed by Endoderma Co., Ltd. (Seongnam, Korea) as a fee-based service following their standardized industrial protocol. The synthesis method of the cross-linked HA particulate and their incorporation into microneedle structures follows the manufacturing protocol previously described by Choi *et al.*,[35] who developed the technology at Endoderma Co., Ltd. (Seongnam, Korea). The preparation of a PMP is based on a combination of microneedle technology and PTT using medical adhesive bandages. The PT microneedles were fabricated using

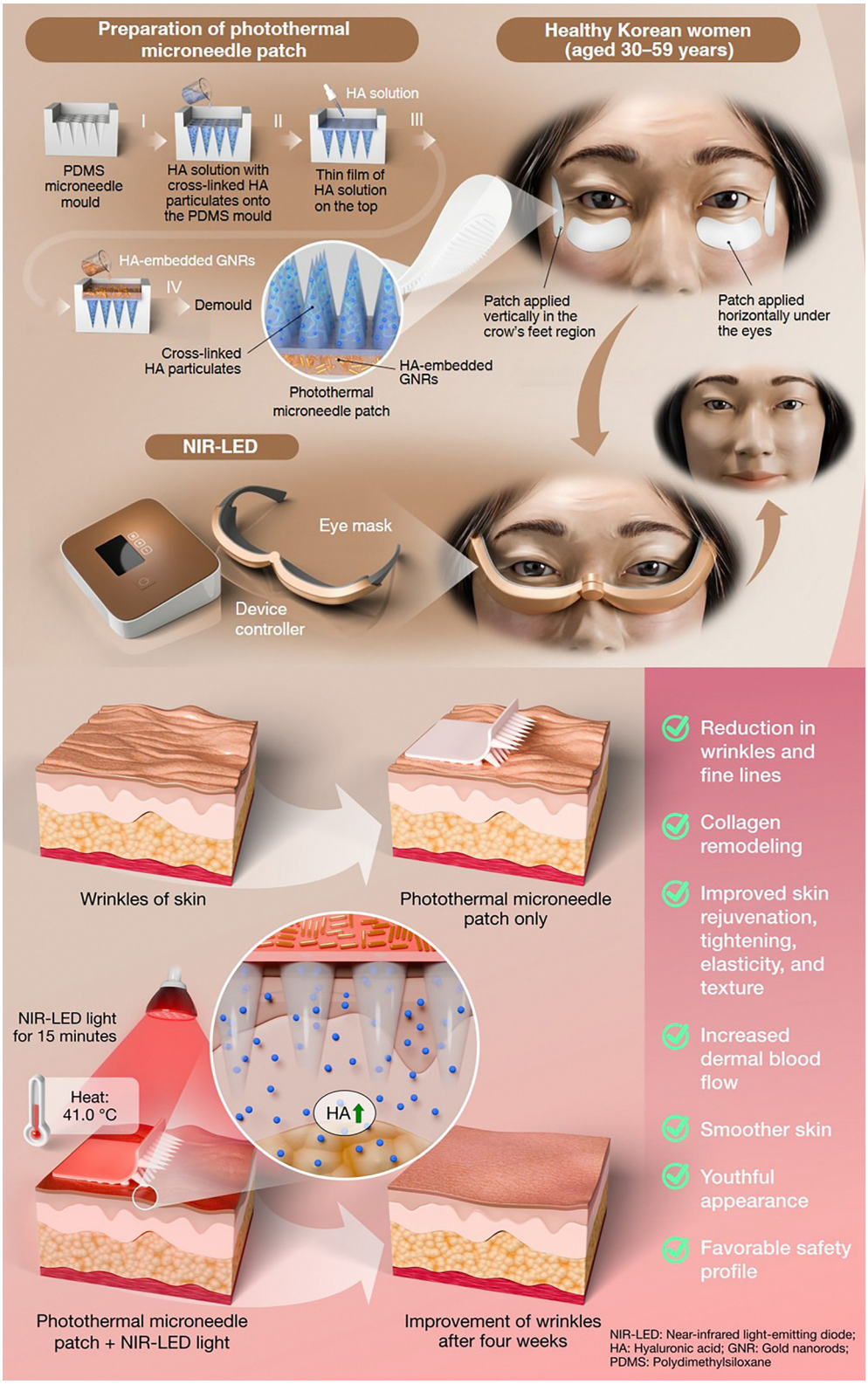

Scheme 1 Photothermal-responsive soluble microneedle eye patch (PMP) and NIR activation. The patch is fabricated using a PDMS microneedle mould by loading a hyaluronic-acid (HA) solution containing cross-linked HA particulates, overcoating with a thin HA film to form dissolvable microneedle tips, and casting a backing embedded with HA–gold nanorod (GNR) complexes, followed by demoulding. In use, patches are placed at the crow's-feet and under the eyes; a wearable eye mask delivers NIR LED light (780 nm, 15 min) to generate mild heat (~41 °C) in the backing, accelerating microneedle dissolution and promoting HA diffusion into the dermis. Repeated use over four weeks is illustrated to reduce wrinkles and smooth skin, consistent with pilot clinical readouts. Abbreviations: NIR-LED, near-infrared light-emitting diode; HA, hyaluronic acid; GNRs, gold nanorods; PDMS, polydimethylsiloxane.

the micromolding method and comprised cross-linked HA particulate-based needle tips and an adhesive hydrocolloid pad based on HA-GNRs. HA solutions with various concentrations were fabricated by combining the HA solution and cross-linked HA particulates at weight ratios of 20 : 80, 40 : 60, 60 : 40, 80 : 20, and 100 : 0 in deionized water (DW) for preparing needle tips with different concentrations of cross-linked HA particles. Additionally, the mixed solution (2.5 mL) was added to the micromold and centrifuged to fill the needle cavity, which was then dried at room temperature for 30 min. The prepared HA solution was first placed on top of a thin film of the adhesive hydrocolloid pad. Then, GNRs were prepared through the seed-mediated growth method reported in our previous work (Korean Patent ''Preparation method of Au nanorod,'' No: 10-1333962)[27,36–38] and GNRs (75 parts per million of gold (ppm of Au)) embedded with the HA solution onto the adhesive back surface of the hydrocolloid pad from Endoderma Co., Ltd. (Seongnam, Korea)[35] through a fee-based manufacturing service according to this established protocol. After drying, the molds were peeled off to obtain PT microneedle arrays. To ensure stability, all patches were vacuum-packaged in moisture-impermeable foil pouches, a standard industrial process used for dissolving microneedle products. Vacuum packaging prevents water uptake and allows long-term storage at room temperature. The company announced that the cross-linked HA microneedle patch was registered and approved by the Food and Drug Administration (FDA) for cosmetic applications. This approved product does not include GNRs. The PMP employed in this study represents a research prototype, and regulatory approval for this modified version is currently being pursued. The fabrication process followed a standardized, previously validated protocol.[35] The physicochemical properties of cross-linked HA particulates, such as crosslinking behaviour, swelling characteristics, and degradation profiles, have been systematically reported in previous studies.[35] In the present study, we focused on the device-level fabrication and functional performance of the PMP system. To further strengthen reproducibility, additional batch-specific characterization of material properties will be included in future studies.

2.4. Morphological analysis

The PMPs were visualized using a Leica S9i stereomicroscope (Leica Microsystems Co. Ltd., Deerfield, IL, USA) to investigate the morphology of the microneedles. The morphological properties and elemental distribution of the PMP were investigated using a field-emission scanning electron microscope (FE-SEM, JSM-IT700HR, JEOL, Japan) equipped with an energy-dispersive X-ray spectrometer (EDX). Transmission electron microscopy (TEM, JEM2100, JEOL, Japan) was used to observe the surface morphology of the GNRs.

2.5. NIR LED light-responsiveness of the PMP

GNRs with varying concentrations (0, 0.1, 1, 5, 10, 30, 50, 75, 100, 150, 200, and 300 ppm of Au) were exposed to 785 nm NIR laser (CNI, MDL-III-785, Changchun, China) irradiation at 0.8 W cm^{-2} for 30 min. The PMP (75 ppm Au) and microneedle patch (0 ppm Au) were placed on a board of NIR LED lights (Epitex, SMBB780D-1100-03, Japan) at a wavelength of 780 nm and exposed to an NIR LED light source for 15 min. The temperature change curves of the PMP were recorded, and an infrared (IR) thermal imaging camera (FLIR CX-Series, Wilsonville, Oregon, USA) continuously captured the real-time temperature of the PMP.

2.6. Tissue-mimicking agarose gel phantom

Agarose gel phantoms for imaging were constructed using 1% agarose powder as the base material by dissolving it in 100 mL of DW. The agarose gel phantom was cylindrical with a diameter and height of 7 and 9.5 mm, respectively. The top of the agarose gel phantom was embedded with or without HA-GNRs, and the diffusion process of methylene blue (MB) solution (10 μL, 0.0125 g mL^{-1}) was added dropwise on the top of the agarose gel phantom.[39,40] A high-power top NIR LED light with a peak wavelength of 780 nm was obtained from Epitex (SMBB780D-1100-03, Japan). An NIR LED light (wavelength of 780 nm) was placed on the top surface of a phantom exposed to the NIR LED light for 15 min for visualizing the dye penetration depth in tissues because of the PT heat energy, which was observed and measured in the MB diffusion inside the agarose gel phantom.

2.7. Intervention

All participants washed their faces and rested at room temperature for 15 min, and were asked to clean their eyes with a hibitane solution and dry the test area well before applying PMP to the area under the eyes and the crow's feet region. All participants were instructed to apply a PMP under the eyes, and a patch was gently pressed onto the under-eye region for 5 seconds, which ensured that the entire surface of the patch was in full contact with the skin for 5 min to enable the needle to penetrate deeply. A wearable NIR LED eye mask device (YOUR NEED79, model CG-001; Freewind, Korea) was used for clinical application. The device delivered NIR light with a peak wavelength of 780 nm (±10%), corresponding to an emission range of approximately 702–858 nm, and operates in multiple modes. It is powered by a built-in rechargeable lithium-ion battery (7.2 V, 3350 mAh) with a maximum output of 20 W. A wearable NIR LED eye mask device was worn over microneedle patches, which were exposed to NIR LED light at 780 nm for 15 min to generate mild heat (PT effect), followed by cooling at room temperature without NIR LED light for 15 min, and then by removing the NIR LED device and patches, whereas PMPs (control) was applied for the same total duration of 30 min without NIR LED light exposure. All participants received moisturizers and were instructed to apply PMPs with NIR LED light for 15 min, three times a week, for a total of four weeks. All participants visited the clinic weekly throughout the study.

2.8. Quantitative evaluation of wrinkle improvement

Periorbital wrinkles, crow's feet wrinkles, and skin roughness were evaluated quantitatively using a small-field PRIMOS^{CR} (Canfield Scientific Inc., USA) equipped with a non-contact

optical three-dimensional (3D) skin imaging device, in which a decrease in R_a (average roughness) values indicates an improvement in wrinkles to measure wrinkle changes. The wrinkle changes in the left and right eyes and the crow's feet region were analyzed using wrinkle analysis parameters. Skin brightness was measured and captured using VISIA-CR (Canfield Scientific Inc., USA) at baseline and at every visit, offering a standard high-resolution facial photography device to identify subsurface skin characteristics. The images captured using VISIA-CR were analyzed using the image analysis software I-MAX Plus (INGPLUS Co., Ltd, Seoul, Korea) to designate the area around the eyes in which an increase in the L^* value indicates an improvement in skin brightness. Images at the same site were captured at each evaluation time point (baseline (zero), two, and four weeks).

2.9. Product preference and safety

All participants were surveyed at every visit for adverse skin reactions, including burning, itching, scaling, prickling, redness, tightness, swelling, erythema, and edema. The efficacy and safety of the application were evaluated at the same site using the same methodology as that used at the initial visit at zero, one, two, and four weeks. In addition to participant-reported symptoms, safety assessments included dermatologist-performed visual examination at each visit to detect any signs of irritation or adverse skin reactions.

2.10. Statistical analysis

The statistical significance of all data was determined using SPSS version 27.0 (SPSS Inc., Chicago, IL, USA). All experiments were performed in at least triplicate ($n \geq 3$) and data were expressed as mean ± standard deviation (SD), with the statistical significance set at $p < 0.05$. Comparison within the population was conducted using the non-parametric Friedman test (*Post hoc*: Wilcoxon signed rank test with Bonferroni correction), parametric test, and repeated-measures analysis of variance (ANOVA) (*Post hoc*: Bonferroni correction).

3. Results and discussion

3.1. Design and fabrication of a PMP

In this study, we developed the first PT-responsive soluble microneedle patch (PMP) as a novel emerging at-home cosmetic product for improving periorbital wrinkles (Scheme 1). The fabrication of PMP combines microneedle technology with PT materials used in medical-adhesive bandages. These PMPs were fabricated using a micromolding technique that contained cross-linked HA particulate-based needle tips and an adhesive back surface of a hydrocolloid pad containing HA-GNRs (Fig. S1). This topology deliberately decouples penetration from actuation: the HA tips ensure painless entry into the upper epidermis, whereas the HA–GNR backing supplies heat without increasing needle length. Localizing Au to the backing (confirmed by EDX) minimizes direct metal–tissue contact while maximizing areal heat transfer to the microneedle–stratum corneum interface.

GNRs have attracted considerable attention as potential PT materials because of their high absorption cross-section for converting NIR light into heat.[27] GNRs were prepared through the widely recognized seed-mediated growth method reported in our previous work (Korean Patent "Preparation method of Au nanorod," No: 10-1333962).[27,36–38] The UV–vis–NIR spectra of the GNRs showed strong absorbance in the NIR region (700–1100 nm) with a high longitudinal surface plasmon resonance (LSPR) band at 803 nm (Fig. S2), which is highly suitable for PTT with NIR light.[41] The TEM image of the GNRs exhibited a uniform rod-like structure with an average length of 51.3 ± 3.1 nm and a diameter of 12.6 ± 4.8 nm, yielding an aspect ratio of 4.07 and resulting in excellent PT properties (Fig. S3).[42]

The PMPs were placed horizontally under the eyes and vertically in the crow's feet region and gently pressed for 5 s to investigate the skin penetration capability of the patches, confirming that the entire surface of the patch was in complete contact with the skin for 5 min because of the deep penetration of the needle. An NIR LED eye mask device emitting light at a wavelength of 780 nm was worn over microneedle patches, which were exposed to the NIR LED light for 15 min to generate mild heat, followed by cooling at room temperature without NIR LED light for 15 min, and then the NIR LED device and patches were removed. All participants were instructed to apply PMPs with NIR LED light for 15 min three times a week for a total of four weeks (Fig. 1a). We investigated the dissolution process of PMPs with or without NIR LED light on the skin by removing the patches at various time intervals and observing them using FESEM to confirm the patch volume changes (Fig. 1b). The morphology of the fabricated PMP (Fig. 1c) was examined using a Leica S9i stereomicroscope and FE-SEM to investigate its specificity and uniformity, particularly the average length and diameter at the base and tip. The stereomicroscopic (Fig. 1d) and FESEM (Fig. 1e) images of the fabricated PMP show a cone shape, smooth surface, and uniform array. The average length and diameter at the base and tip of the PMP were 265, 90, and 6 μm, respectively. The ~265 μm height targets the viable epidermis without bleeding; ~6 μm tips lower insertion force and favor rapid dissolution once hydrated, while the dense arrays (under-eye 850 ± 6; crow's-feet 530 ± 5) increase total heat-exchange area. The average length of 265 μm microneedles was selected because it is painless. The total number of microneedles, strength, size, weight, and pH of the patch for periorbital wrinkles were 850 ± 6, 0.25 N, 346.4 mm^2, 21 mg, and 7.1, and the total number of microneedles, strength, size, weight, and pH of the patch for the crow's feet wrinkles were 530 ± 5, 0.25 N, 211.3 mm^2, 14.8 mg, and 7.1, respectively. Two PMPs for periorbital wrinkles and the crow's feet region were packed into a single plastic box for ease of use during the human pilot clinical trial and applied thrice a week for a total of four weeks. Additionally, FESEM-EDX mapping was performed to visualize HA-GNRs on the adhesive back surface of the hydrocolloid pad, which indicated that Au, C, and O were uniformly distributed on the adhesive back surface of the hydrocolloid pad

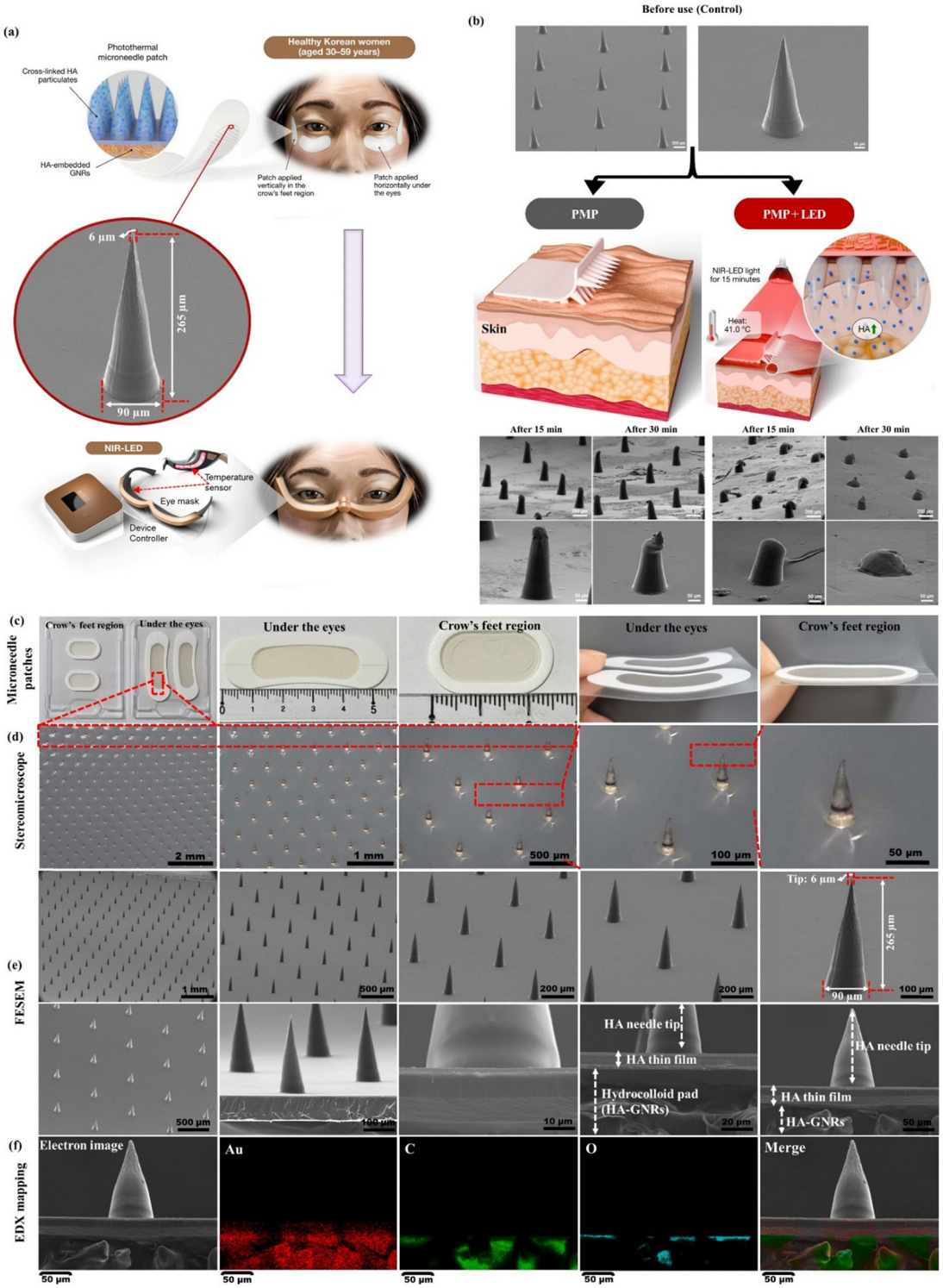

Fig. 1 Application of a photothermal microneedle patch (PMP) and NIR–accelerated dissolution. (a) PMP is designed for the periorbital region. A representative FESEM image shows conical microneedles (height ~265 μm, base ~90 μm, tip radius ~6 μm). Patches are placed horizontally under the eyes and vertically at the crow's-feet and irradiated using a wearable eye mask with an NIR-LED (780 nm) and temperature sensing. (b) Field-emission scanning electron micrographs of microneedles before use and after 15 or 30 min of application with or without NIR-LED irradiation. NIR-LED exposure produces mild heating (~41 °C) and accelerates dissolution, yielding greater tip blunting and loss of microneedle height by 30 min than the non-irradiated control. Scale bars, 200 μm (arrays) and 50 μm (single needles). (c) Photographs of patches tailored for the under-eye and crow's-feet regions. (d) Stereomicroscope images showing uniform microneedle arrays with enlarged views of individual tips. (e) Field-emission SEM images of arrays and cross-sections; dissolvable HA microneedle tips (~265 μm height, ~90 μm base, ~6 μm tip radius) are formed on a thin HA film supported by a hydrocolloid pad containing HA–gold nanorod (HA–GNR) composites. (f) Energy-dispersive X-ray (EDX) elemental maps across a cross-section, confirming Au localization within the backing layer (from HA–GNRs) and the distribution of C and O in the HA matrix. Scale bars as indicated. Data are presented as means ± SD (n = 3 independent experiments).

(Fig. 1f). The microneedle tips and top of the thin film of the adhesive hydrocolloid pad were in direct contact with the skin, which did not have GNRs, demonstrating that HA-GNRs were successfully fabricated on the back surface of the hydrocolloid pad. The results demonstrated that the PT microneedle tips began to dissolve after patch insertion, dissolved more than three-quarters when exposed to NIR LED light for 15 min, and almost fully dissolved after 30 min of application, remaining embedded within the tissue, whereas PMPs only exhibited slight dissolution in the microneedle tip (33%) after 30 min of application (Fig. S4). These results confirm that NIR LED light exposure enhanced the solubility of the microneedle tips because of the PT effect of the GNRs. Additionally, the PT microneedle tip penetration depth was ~90% of the 265 μm length after patch attachment under the eyes and crow's feet region; the penetrating PT microneedle tip was completely dissolved by bodily fluids and PT effects for further increasing the dissolution rate after 30 min of application because the short length is painless and can make contact with the surface of the skin more closely. The microchannels formed by microneedle insertion are temporary and generally reseal within a few hours owing to rapid skin barrier recovery, thereby reducing the risk of infection or prolonged skin disruption. Similar findings have been reported, which showed that the length of the microneedle tip was 280 μm and microneedle tip penetration was ~92%.[43] Therefore, the recommended application time for clients using PMPs is 30 min to optimize product consumption.

3.2. Photothermal actuation and accelerated dissolution under NIR-LED irradiation

GNRs are excellent candidates for PTT because of their high PT conversion efficiency and PT stability, which can generate mild-to-high temperatures within a short NIR laser irradiation time.[44] An NIR laser (wavelength 785 nm) is considered the most suitable light source for PTT because of its advantageous characteristics, including deeper tissue penetration, low absorbance by blood, water, and biological tissues, and few adverse effects.[45] The PT effects generated by irradiating GNRs at different concentrations (0, 0.1, 1, 5, 10, 30, 50, 75, 100, and 150 ppm of Au) with a 785 nm NIR laser at 0.8 W cm^{-2} for 30 min exhibited a concentration-dependent temperature change (Fig. 2a). More interestingly, the temperature of the GNRs (75 ppm of Au) quickly increased from 30.24 to 43.08 °C, where a mild temperature was more attractive and practical for PTT, whereas it only marginally increased to 32.02 °C in DW.

The eyelid skin is extremely sensitive to temperature changes because of its exceptionally thin and densely innervated structure. The NIR LED device controller and eye mask with a temperature sensor are used in clinical settings for managing eye protection, which provides precisely controlled heat at ~41.0 °C, indicating that the temperature is considered safe for eyelid warming.[21,46] The NIR LED device was equipped with an internal surface temperature sensor integrated into a closed-loop feedback system that continuously adjusted the LED output to maintain a stable temperature of approximately 41.0 °C at the mask-patch interface. In our fabricated patches, the temperature changes in the PMPs were accurately controlled by the concentration of GNRs (75 ppm of Au). Furthermore, PMP (75 ppm of Au) and microneedle patches (0 ppm of Au) were placed on board an NIR LED light at a wavelength of 780 nm and exposed to an NIR LED light source for 15 min to investigate the PT effect of microneedle patches (Fig. 2b). At the patch surface, the NIR LED delivered an irradiance of 2.33 mW cm^{-2} over an illuminated area of approximately 6.0 cm^2 per side, with a mask–skin distance ~2 mm, establishing a reproducible mild-thermal dose. The real-time temperature change curves of the PMP (75 ppm of Au) were recorded using an IR thermal imaging camera with a microneedle patch (0 ppm of Au) as a control. The temperature of the PMP (75 ppm Au) rapidly increased from 34.59 to 41.01 °C; however, the temperature of the microneedle patch only (0 ppm Au) showed a slight change from 34.45 to 35.86 °C after switching the NIR LED light on for 15 min (Fig. 2c). The IR thermal images of the temperature changes in the patches are shown in Fig. 2d. Operating near 41 °C places the system in a mild-thermal regime that (i) lowers HA viscosity at the tip–stratum corneum interface, (ii) increases water flux from the hydrocolloid, and (iii) accelerates microneedle dissolution, consistent with FESEM showing >75% tip loss at 15 min and near-complete dissolution by 30 min with NIR, *versus* ~33% without light. During human sessions, patch-surface temperature was monitored by the mask sensor and confirmed by IR thermography, maintaining ~41 °C throughout exposure. The applied PT (~41.0 °C for 15 min) corresponds to a negligible thermal dose relative to established tissue damage thresholds (*e.g.*, cumulative equivalent minutes at 43.0 °C (CEM43)), thereby supporting the safety of the treatment, even in sensitive periorbital skin. The PT effect rapidly increased skin temperature to ~41.0 °C, enhancing the fluidity of the epidermal lipid layer, which improved the transdermal absorption rate of anti-wrinkle agents. We hypothesized that a PMP could promote rapid heating to a skin temperature of ~41.0 °C within 15 min in human clinical trials, starting from the normal human basal body temperature (36.5–37.5 °C).

3.3. Tissue-phantom studies indicate deeper dye transport with NIR-activated patches

Biological tissue-mimicking phantoms have been proposed as artificial models to simulate biological organs and study the physicochemical impacts on the human body. The agarose gel phantom is appropriate because it mimics the target tissue and is inexpensive to prepare.[47,48] MB can be used to monitor the diffusion processes occurring within an agarose gel phantom to simulate the real processes occurring in living tissues. Agarose gel phantoms were successfully created using 1% agarose powder, which was investigated for PT heat generation and diffusion (Fig. 3). The phantom was cylindrical and measured 7 mm in diameter and 9.5 mm in height. The top of the phantom was embedded with or without HA-GNRs, and MB was applied dropwise to the top of the phantom during the diffusion. The NIR LED light (780 nm) was exposed on top of the surface phantom for 15 min to visualize the depth of dye

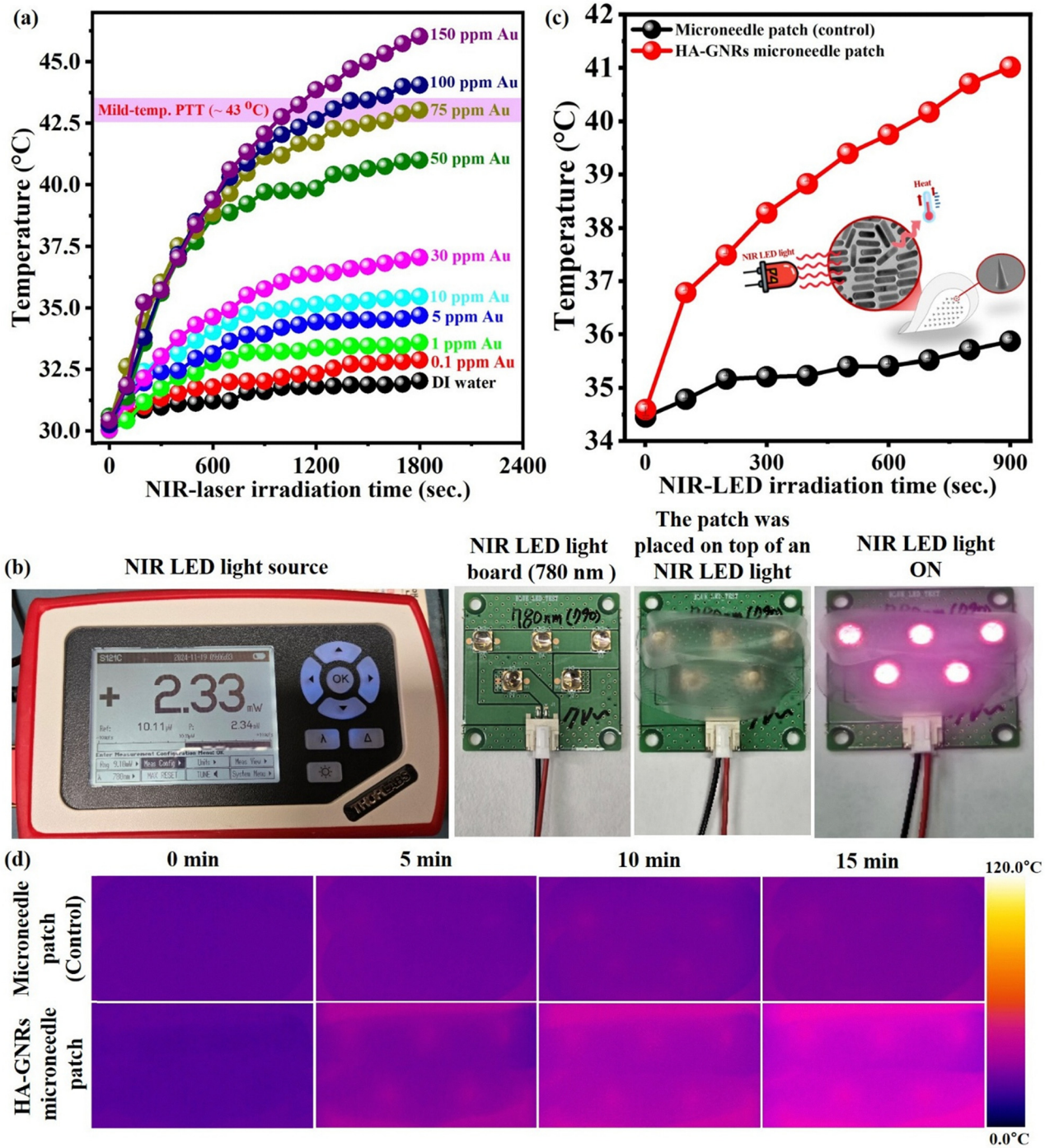

Fig. 2 Photothermal response of gold-nanorod–integrated microneedle patches under NIR illumination. (a) Temperature–time profiles of aqueous GNR dispersions (0.1–150 ppm Au) under NIR-laser irradiation (up to 1800 s); the horizontal line marks the mild-photothermal range (~43 °C). (b) Experimental setup: a wearable NIR-LED light source and a 780 nm LED board; a microneedle patch placed on the board and shown with the LEDs on. (c) Heating curves of the HA–GNR microneedle patch *versus* a control microneedle patch without GNRs during 780 nm NIR-LED irradiation for 15 min. (d) Infrared thermography at 0, 5, 10, and 15 min showing stronger warming of the HA–GNR patch relative to the control. Data are presented as means ± SD (n = 3).

penetration in tissues because of the PT heat energy, which was measured by the MB diffusion inside the phantom. NIR-activated HA–GNR layers approximately doubled the dye-front depth (≈5.1 mm *vs.* ≈2.6 mm at 15 min), indicating heat-augmented diffusion/micro-convection in hydrated gels and providing a mechanistic bridge from faster on-skin dissolution to enhanced perichannel transport. Notably, this increase in penetration depth cannot be explained by thermal diffusion alone; rather, it likely

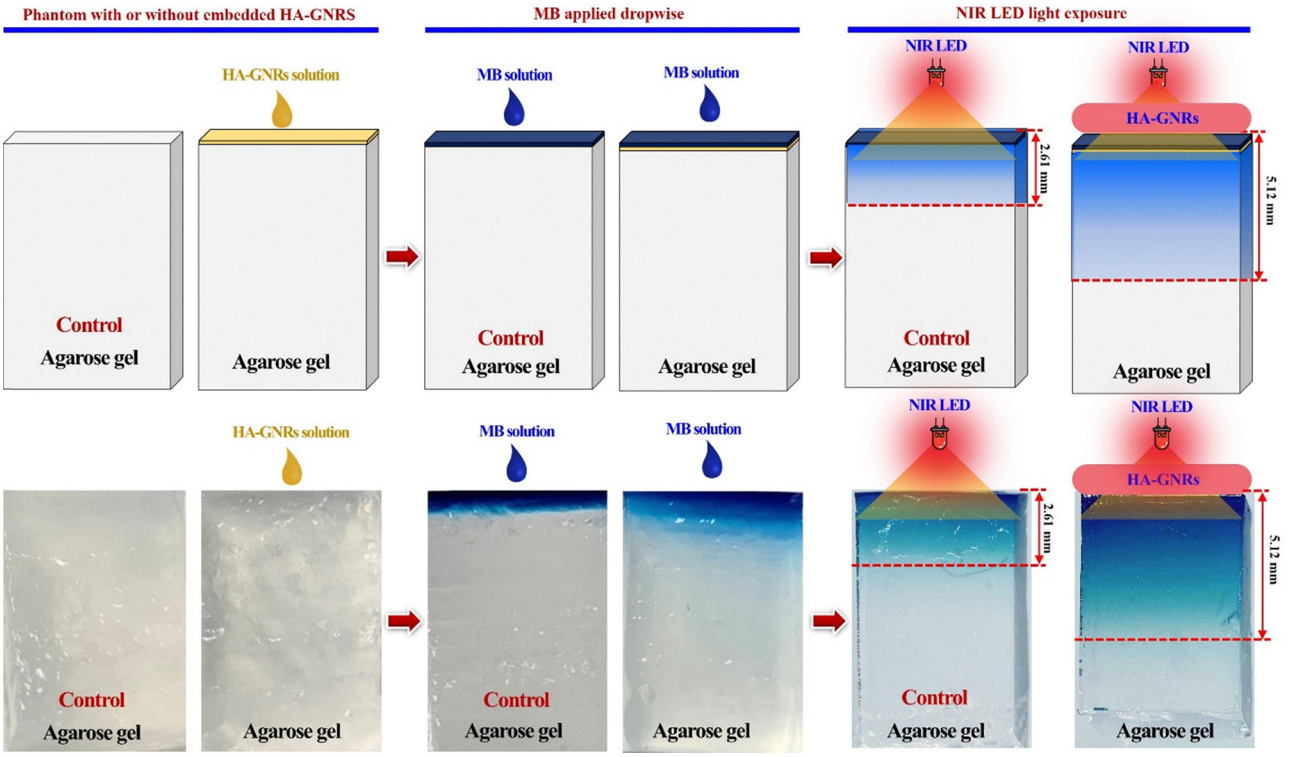

Fig. 3 Penetration depth of PT heating and dye diffusion in agarose-gel phantoms. Agarose blocks were prepared without (control) or with a surface layer containing HA–GNRs. A methylene-blue (MB) solution was applied to the top surface, and the gels were irradiated from above with an NIR LED (≈780 nm). Schematics and photographs show that photothermal heating from HA–GNRs increased the downward diffusion/convective transport of MB, shifting the visible front (red dashed line) from ∼2.6 mm in the control to ∼5.1 mm with HA–GNRs. Representative images from independent experiments (n = 3).

arises from a combination of localized photothermal gradients, hydrogel softening, and swelling-driven microconvective transport within the hydrated matrix. The temperature increase in the gel phantom embedded with HA-GNRs and diffusion of MB into the gel phantom at a depth of dye penetration was 5.12 mm, indicating that the PT effect of HA-GNRs with NIR LED light can increase the molecular diffusion rate by more than two times; all molecules move because of their PT heat energy, causing diffusion. Conversely, the diffusion of MB into the gel phantom (control) with NIR LED light at the depth of dye penetration was 2.61 mm, suggesting that PT agents were absent in the control. These findings indicate that HA-GNRs exposed to NIR LED light exhibit deeper penetration of light into tissues, which is useful for clinical diagnosis.

3.4. Pilot randomized clinical evaluation of periorbital wrinkle reduction

Twenty healthy Korean women who visited the participating clinics between November 2021 and January 2022 were enrolled in the study. There were no contraindications for applying PMP in any of the participants. The average age of the 20 participants was 50.1 ± 6.3 years (mean ± SD), and all participants had mild-to-moderate periorbital wrinkles according to the modified Lemperle wrinkle assessment scale.[49] Furthermore, two people (10%) were in their 30–39 s, six people (30%) were in their 40–49 s, and twelve people (60%) were in their 50–59 s. A total of 20 participants completed the follow-up period and exhibited significant improvements in their periorbital wrinkles (Fig. 4a). Periorbital wrinkles, the crow's feet region, and skin roughness were analyzed using a small-field PRIMOS^{CR}. The prespecified primary endpoint was percentage change in PRIMOS R_a under the eye from baseline to week 4; secondary endpoints included crow's-feet R_a, VISIA-CR L, and melanin value. Table S1 provides information on the R_a measurements of periorbital wrinkles using PRIMOS. The R_a value was 28.147 ± 8.352 prior to use. The R_a value measurement of periorbital wrinkles grading exhibited a statistically significant decrease in the first, second, and fourth weeks with a mean difference of 8.658% (Mean ± SD: 25.602 ± 7.889, p <0.001), 13.598% (Mean ± SD: 24.147 ± 7.572, p <0.001), and 16.336% (Mean ± SD: 23.417 ± 7.375, p <0.001), respectively, indicating that the fourth week showed more improvement than other weeks (Fig. 4b and c). The monotonic 8.7% → 13.6% → 16.3% R_a reductions argue against transient smoothing alone and are consistent with cumulative benefit from repeated, heat-assisted dissolution and short-range HA/water transport into microchannels. These results suggest that the PMP with NIR LED light for periorbital wrinkles improved by more than twice that of general microneedle patches. The greatest individual improvement (∼50% reduction in R_a) was observed in a single participant, with a representative example shown in Fig. 4a, highlighting the

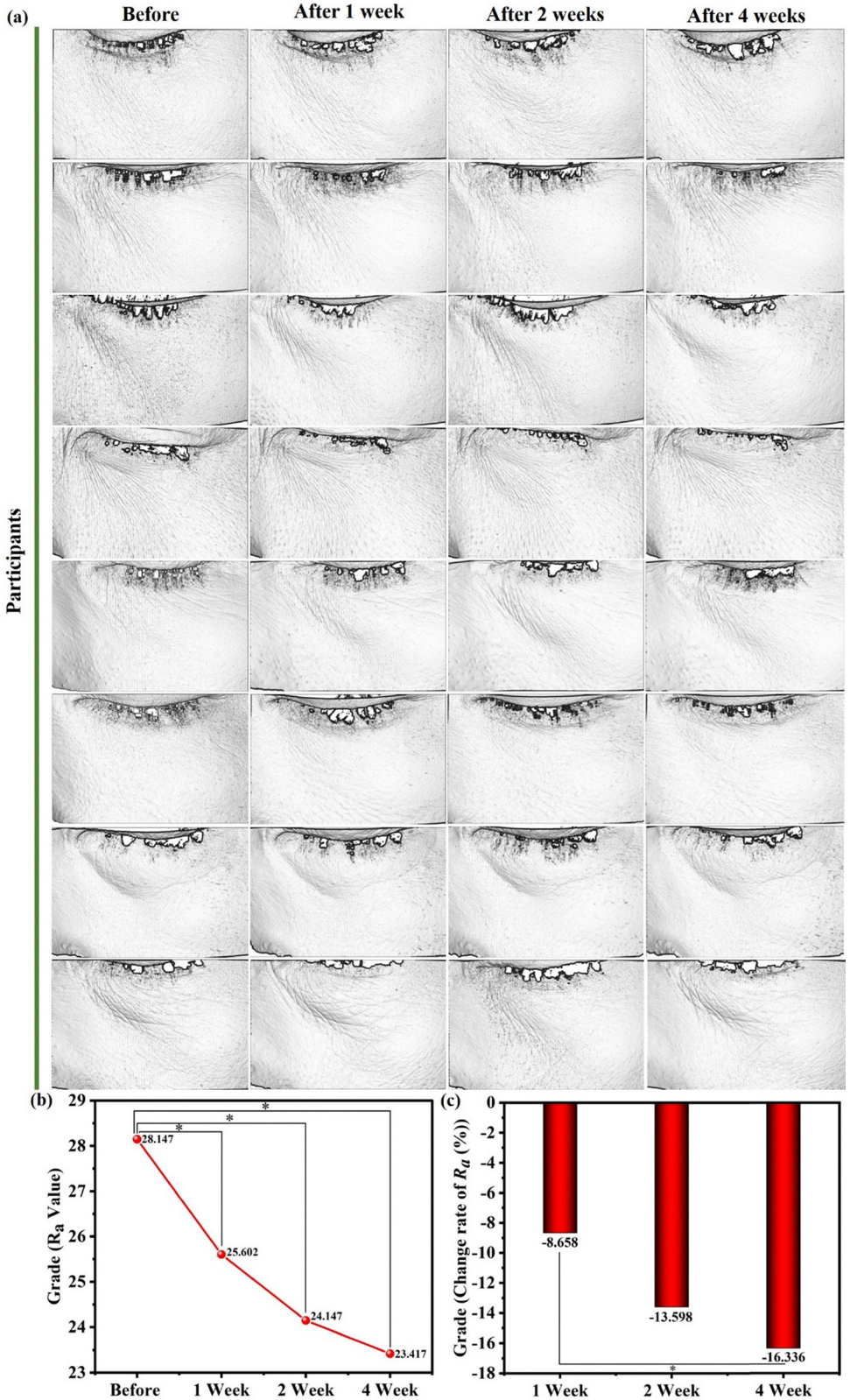

Fig. 4 Longitudinal PRIMOS assessment of periorbital wrinkles during treatment with a PMP and NIR LED. (a) PRIMOS topography images of the under-eye region from representative participants at baseline and after 1, 2, and 4 weeks of treatment with the PMP plus NIR LED (NIR-LED) irradiation, showing progressive attenuation of wrinkle features. (b) PRIMOS average roughness (R_a) values across the same time points, indicating a steady decrease from baseline. (c) Percentage change in R_a relative to baseline at 1, 2, and 4 weeks. Statistical analysis used the Friedman test with post-hoc Wilcoxon signed-rank tests and Bonferroni correction; * denotes corrected $p < 0.05$. Data are presented as means ± SD (n = 20 participants).

potential efficacy of the treatment. A limitation of this experiment is the lack of a thermal control group (*e.g.*, a simple ~41.0 °C warm compress without GNRs). Consequently, the relative contributions of general heating and the specific PT effect of GNRs could not be fully separated. Further studies will incorporate appropriate thermal control conditions to clarify these effects.

3.5. NIR-LED enhances crow's-feet outcomes *versus* the patch alone

In a with-/without-NIR comparison at the crow's-feet (ides were randomized 1 : 1 to PMP + NIR-LED or PMP only, with allocation concealed and PRIMOS analysis blinded to side), NIR-LED increased the mean improvement in wrinkle grade to ~14.1% at week 4 *versus* ~1.9% without NIR (≈7-fold difference), with representative PRIMOS images illustrating greater ridge attenuation under NIR-LED, matching the expected effect of faster dissolution and enhanced post-insertion transport with heating (Fig. 5 and Fig. S5). Briefly, PMPs were applied the crow's feet region and then exposed with or without NIR LED light for 15 min (Fig. 5). The effect of PMP with NIR LED light in the crow's feet region was 14.1% higher than that of PMP without NIR LED light, suggesting that the effect of PMP with NIR LED light in the crow's feet region was more than seven times higher than that of the microneedle patch without NIR LED light. A 53-year-old woman with the best outcomes showed a 46% improvement in the appearance of crow's feet wrinkles (Fig. S5).

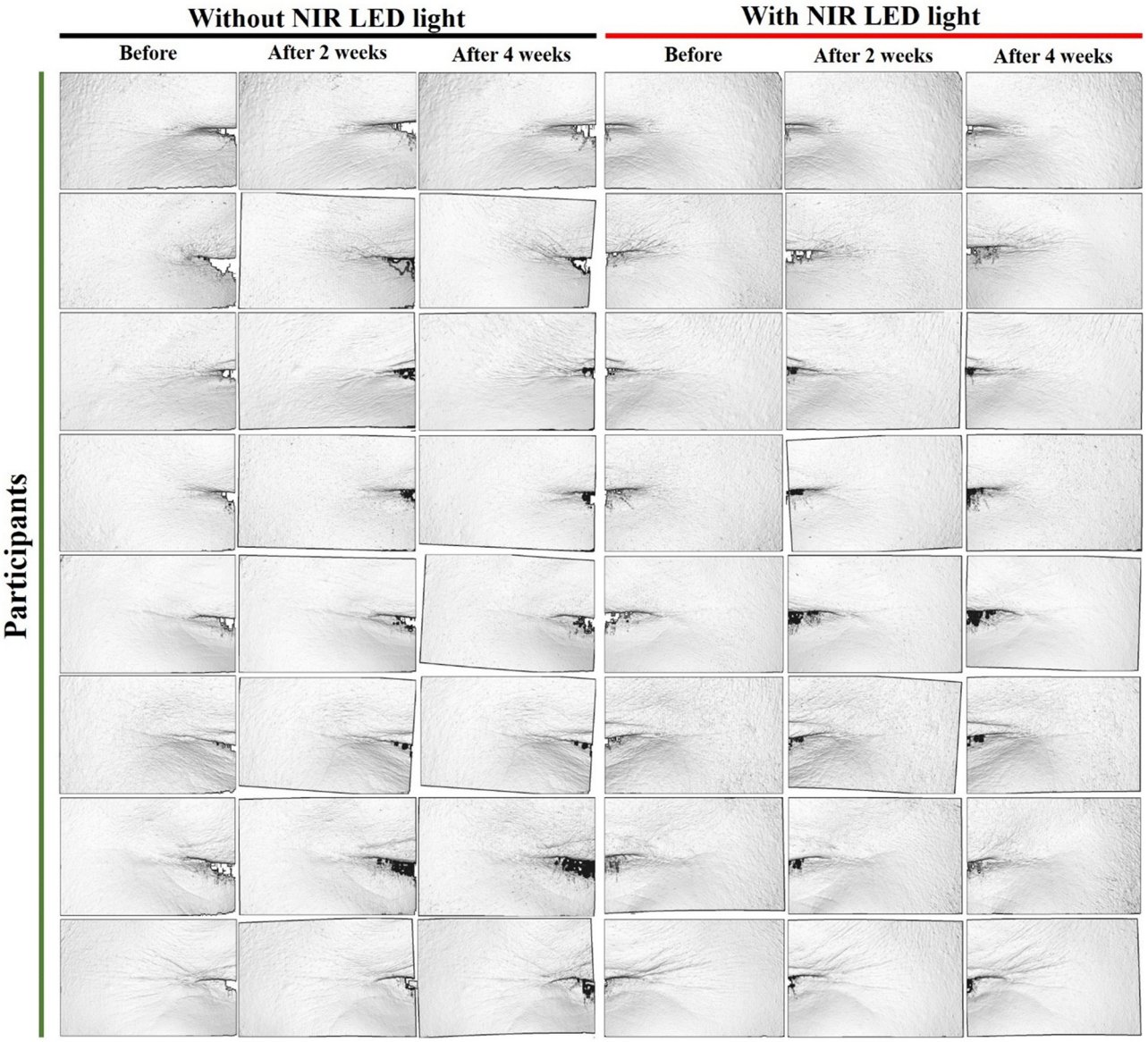

Fig. 5 NIR illumination enhances wrinkle improvement with a PMP. PRIMOS topography images of crow's-feet from representative participants treated with the PMP either without NIR-LED (left; baseline, week 2, week 4) or with NIR-LED (right; baseline, week 2, week 4). The addition of NIR-LED is associated with a more pronounced attenuation of wrinkle ridges over 4 weeks than PMP alone. Data are presented as means ± SD (n = 20 participants).

Fig. 6 Representative VISIA-CR photographs showing brightening of the periorbital area during treatment. Clinical images from representative participants captured with VISIA-CR at baseline and after 1, 2, and 4 weeks of treatment with the PMP plus NIR LED (NIR-LED) irradiation. The sequences illustrate progressive lightening of the under-eye region; quantitative analysis of VISIA-CR brightness (L^*) showed a significant increase by week 2 that persisted through week 4. Data are presented as means ± SD (n = 20 participants).

3.6. Skin brightness increases and facial melanin decreases with NIR activation

Skin brightness was measured using a VISIA-CR system (Fig. 6). Table S2 presents the L^* value measurements of skin brightness around the eyes using VISIA-CR. The skin brightness L^* value was 72.438 ± 3.069 before use, and the skin brightness L^* value was significantly increased in the first, second, and fourth weeks with a mean difference of 1.201% (Mean ± SD: 73.308 ± 2.990, $p < 0.008$), 1.979% (Mean ± SD: 73.847 ± 2.568, $p < 0.001$), and 1.462% (Mean ± SD: 73.488 ± 3.183, $p < 0.007$), respectively, resulting in significantly more improvement in skin brightness (Fig. S6a and b). Additionally, PMPs were placed under the eyes and in the crow's feet region and exposed with or without NIR LED light for 15 min (Fig. S7). The skin melanin changes and improvement of skin whitening effect of PMP with NIR LED light were found to be 7.29% compared to those of PMP without NIR LED light (2.83%), indicating that skin melanin-pigmented spots gradually improved the lightness of skin color from baseline (zero weeks) to four weeks for PMP with NIR LED light (Fig. S8). The increase in skin brightness is mainly associated with improved hydration and smoothing of the skin surface, which enhances light reflectance. The additional effect observed under NIR LED light may be related to increased local microcirculation and epidermal turnover rather than direct suppression of melanogenesis.

No adverse effects on the eyes or skin, such as burning, itching, scaling, prickling, redness, tightness, swelling, erythema, or edema, were reported by any participant throughout the study. No abnormal skin symptoms were detected during the physical examination by the dermatologist. In the survey of PMPs with NIR LED light preference, all participants (100%) responded "no" when asked to feel the pain and redness induced by PMPs with NIR LED light. All twenty participants completed the protocol with no device-related adverse events and no reports of pain or redness during sessions, supporting at-home feasibility with the current thermal limits. These findings indicate that PMPs irradiated with NIR LED light are safe for use in cosmetics. These findings, integrating both participant-reported outcomes and dermatologist evaluations, suggest that PMP with NIR LED light treatment is well tolerated and demonstrates a favourable safety profile under the applied conditions. This study was limited by the lack of a mechanistic evaluation of wrinkle improvement. Future studies will include systematic animal experiments and histological analyses to investigate collagen remodeling, epidermal regeneration, and the associated molecular pathways induced by microneedle-assisted photothermal treatment.

4. Conclusions

NIR–actuated microneedle patches combine a dissolving tip for painless penetration with a photothermal backing that supplies a repeatable, eyelid-safe thermal micro-dose, resulting in a significant reduction of wrinkles, creating smoother skin, and achieving a more youthful appearance. In this pilot trial, the system improved under-eye R_a and crow's-feet roughness and increased skin brightness, with zero device-related adverse events. Together with phantom studies showing heat-enhanced transport, the data support a mechanism in which mild heating (~41 °C) accelerates tip dissolution and augments short-range mobility of HA and interstitial water through combined diffusion, hydrogel softening, and micro-convective effects, producing immediate topographic smoothing.

Translationally, the architecture decouples penetration from actuation, allowing multiple control knobs, Au loading, LED irradiance/duty cycle, wear time, and hydrocolloid water activity to tailor thermal dose without altering needle geometry. Reporting irradiance and thermal dose will enable cross-study comparison and model-based optimization. The same platform could deliver other hydrophilic actives (for example, peptides) or pair with closed-loop temperature control using the existing mask sensor to personalize heating by skin type.

Future trials should (i) incorporate dose–response arms (Au concentration and irradiance), (ii) stratify by Fitzpatrick type and age to understand responders, (iii) extend follow-up to quantify durability and rebound, and (iv) include patient-reported outcomes and quality-of-life measures aligned with cosmetic benefit. A multi-site, adequately powered study with pre-registered endpoints (R_a, L^*, melanin) and effect sizes with 95% CIs will meet community standards for evidence and facilitate regulatory and commercial translation.

From a manufacturability perspective, the micromoulding plus hydrocolloid process is compatible with roll-to-roll production, and gold loadings in the tens of ppm range suggest a favorable cost and environmental footprint. Careful end-of-life handling and recycling of Au from backing laminates could further improve sustainability.

Author contributions

Hyo-Won Han: methodology, investigation, data curation, formal analysis. Dong-Hwan Lee: conceptualization, resources, formal analysis, investigation. Ara Joe: project administration, data curation, software, validation. Yeong Jun Jeon: visualization, data curation, formal analysis. Yu-Ra Lim: methodology, software, formal analysis. Sang Bong Lee: conceptualization, methodology, resources. Bum-Ho Bin: conceptualization, resources, methodology, formal analysis. JuKyung Lee: resources, data curation, conceptualization, software. Thavasyappan Thambi: software, investigation, methodology, data curation. João Conde: supervision, resources, funding acquisition, visualization, writing – review and editing. Panchanathan Manivasagan: conceptualization, investigation, writing – original draft. Eue-Soon Jang: supervision, validation, resources, funding acquisition, writing – review and editing.

Conflicts of interest

J. C. is a co-founder and shareholder of TargTex S. A. – Targeted therapeutics for Glioblastoma Multiforme. J. C. is a member of the Global Burden Disease (GBD) consortium of the Institute

for Health Metrics and Evaluation (IHME), University of Washington (US), and is on the Scientific Advisory Board of Vector Bioscience Cambridge. The other authors have no conflicts of interest to declare.

Data availability

The supporting data for this study are provided in the supplementary information (SI). Supplementary information: Fig. S1. Fabrication of a photothermal-responsive soluble microneedle eye patch. Fig. S2. UV–vis–NIR absorption of gold nanorods and overlap with the excitation source. Fig. S3. Transmission electron microscopy (TEM) of gold nanorods. Fig. S4. Near-infrared illumination accelerates dissolution of the photothermal microneedle patch. Fig. S5. Crow's-feet wrinkle improvement with and without near-infrared illumination. Fig. S6. Brightening of the periorbital skin during treatment with a photothermal microneedle patch and near-infrared LED. Fig. S7. Reduction of facial pigmentation with a photothermal microneedle patch, with and without near-infrared illumination. Fig. S8. Reduction in facial melanin with a photothermal microneedle patch, with and without near-infrared illumination. Table S1. Measure the results of wrinkles around the eyes using PRIMOS. Table S2. Measure the results of skin brightness using VISIA-CR. See DOI: https://doi.org/10.1039/d6tb00534a.

Acknowledgements

E.-S. J. gratefully acknowledges partial financial support from the Korean Ministry of Education, Science & Technology under grants 2016R1D1A3B0201175615 and RS-2026-25475964513820706700001 (contributions: 10% and 30%, respectively); the Korean Health Technology R&D Project through the Korea Health Industry Development Institute (KHIDI), funded by the Ministry of Health and Welfare, under grants HP23C0260 and RS-2025-02263897 (contributions: 20% and 20%, respectively); and the Innovative Human Resource Development for Local Intellectualization Support Program, supervised by the Institute of Information & Communications Technology Planning & Evaluation (IITP), under grant IITP-2026-RS-2020-II201612 (contribution: 20%). J. C. is incredibly grateful for the research grant from the Regional Innovation System & Education (RISE) program of Gyeongsangbuk-do, Republic of Korea.

Notes and references

1 M. Yaar, M. S. Eller and B. A. Gilchrest, *J. Invest. Dermatol. Symp. Proc.*, 2002, **7**, 51–58.
2 Y. Ma, C. Li, Z. Mai, J. Yang, M. Tai and G. Leng, *J. Cosmet., Dermatol.*, 2022, **21**, 3496–3502.
3 Q. Qu, Z. Cui, F. Jiang and C. Liu, *J. Drug Delivery Sci. Technol.*, 2024, **100**, 106065.
4 L. Baumann, *J. Pathol.*, 2007, **211**, 241–251.
5 Y. Jung, E. Kim, J. Cho, K. Suh and G. Nam, *J. Eur. Acad. Dermatol. Venereol.*, 2013, **27**, e328–e332.
6 S. M. Ali and G. Yosipovitch, *Acta Derm.-Venereol.*, 2013, 93.
7 J. I. Lee, S. J. Kang and H. Sun, *Arch. Plast. Surg.*, 2017, **44**, 340–343.
8 S. Peter and S. Mennel, *Clin. Exp. Ophthalmol.*, 2006, **34**, 363–364.
9 F. Bachmann, R. Erdmann, V. Hartmann, L. Wiest and B. Rzany, *Dermatol. Surg.*, 2009, **35**, 1629–1634.
10 B. J. Kim, H. J. You, I. Jung and D. W. Kim, *J. Cosmet., Dermatol.*, 2020, **19**, 1307–1310.
11 A. Lucaciu, P. F. Samp, E. Hattingen, R.-I. Kestner, P. Davidova, T. Kohnen, J. Rudolph, A. Dietz, H. Steinmetz and A. Strzelczyk, *Neurol. Res. Pract.*, 2022, **4**, 40.
12 A. Arepagorn, J. Meephansan, P. Sirithanabadeekul, K. Tantisantisom, S. Thongma, Y. Rayanasukha, T. Boonkoom and P. Khanchaitit, *Cosmetics*, 2024, **11**, 92.
13 J. Chen, C. Liufu, W. Zhang, C. Luo, K. Fu, J. Lin, J. Liang, W. Yang, F. Song and F. Yang, *Int. J. Cosmetic Sci.*, 2024, **46**, 209–227.
14 Z. Ismail, M. S. Affandi Yusoff and K. Hashim, *J. Dispersion Sci. Technol.*, 2009, **30**, 68–71.
15 X. Zhang, W. Wang, M. Zhu and D. Yu, *J. Text. Inst.*, 2018, **109**, 1536–1542.
16 S. H. Lim, W. J. Tiew, J. Zhang, P. C.-L. Ho, N. N. Kachouie and L. Kang, *Biofabrication*, 2020, **12**, 035003.
17 X. He, J. Sun, J. Zhuang, H. Xu, Y. Liu and D. Wu, *Dose Response*, 2019, **17**, 1559325819878585.
18 M. T. McCrudden, E. McAlister, A. J. Courtenay, P. González-Vázquez, T. R. Raj Singh and R. F. Donnelly, *Exp. Dermatol.*, 2015, **24**, 561–566.
19 T. T. Nguyen and J. H. Park, *Expert Opin. Drug Delivery*, 2018, **15**, 235–245.
20 Y. Cong, H. Li, A. K. Pandya, L. K. Vora, Y. Li, F. Volpe-Zanutto, A. J. Paredes, A. M. Abraham, J. Gao and E. Larrañeta, *Mater. Today Adv.*, 2025, **28**, 100650.
21 F. Yu, X. Zhao, Q. Wang, Y. Niu, P. Xiao, J. Zhang, K. Fei, Y. Huang, L. Liu and P. H. Fang, *Adv. Sci.*, 2025, 2413962.
22 J. H. An, H. J. Lee, M. S. Yoon and D. H. Kim, *Ann. Dermatol.*, 2019, **31**, 263.
23 E. Papakonstantinou, M. Roth and G. Karakiulakis, *Derm.-Endocrinol.*, 2012, **4**, 253–258.
24 G. D. Prestwich, D. M. Marecak, J. F. Marecek, K. P. Vercruysse and M. R. Ziebell, *J. Controlled Release*, 1998, **53**, 93–103.
25 P. Manivasagan, S. W. Jun, N. T. P. Truong, G. Hoang, S. Mondal, M. S. Moorthy, H. Kim, T. T. V. Phan, V. H. M. Doan and C.-S. Kim, *J. Mater. Chem. B*, 2019, **7**, 3811–3825.
26 Y. Cheng, Q. Chen, H. Wang, L. Zhang and J. Zhu, *Macromol. Biosci.*, 2025, e00158.
27 A. Joe, P. Manivasagan, J. K. Park, H.-W. Han, S.-H. Seo, T. Thambi, V. H. Giang Phan, S. A. Kang, J. Conde and E.-S. Jang, *ACS Nano*, 2024, **18**, 19581–19596.
28 W. Zhang, L. Cai, J. Gan and Y. Zhao, *Smart Med.*, 2024, **3**, e20240007.
29 S. Dong, Y. Zhang, Y. Zhang, Y. Mei, A. Sina, R. Zou and L. Niu, *J. Nanobiotechnol.*, 2024, **22**, 199.

30 A. Zhang, X. Jiang, B. Xiong, J. Chen, X. Liu, S. Wang, B. Li, M. Peng and W. Li, *Adv. Sci.*, 2025, **12**, e03698.
31 F. Yu, X. Zhao, Q. Wang, Y. Niu, P. Xiao, J. Zhang, K. Fei, Y. Huang, L. Liu and P. H. Fang, *Adv. Sci.*, 2025, **12**, 2413962.
32 K. Chen, X. Sun, Y. Liu, S. Li and D. Meng, *Front. Pharmacol.*, 2025, **16**, 1607210.
33 T. Peng, Y. Chen, X. Luan, W. Hu, W. Wu, B. Guo, C. Lu, C. Wu and X. Pan, *Bioact. Mater.*, 2025, **45**, 274–300.
34 D. Jang, J. Shim, D. M. Shin, H. Noh, S. J. Oh, J. H. Park and J. H. Lee, *Dermatol. Ther.*, 2022, **35**, e15732.
35 J.-T. Choi, S.-J. Park and J.-H. Park, *J. Drug Targeting*, 2018, **26**, 884–894.
36 N. R. Jana, L. Gearheart and C. J. Murphy, *J. Phys. Chem. B*, 2001, **105**, 4065–4067.
37 H.-W. Han, A. Joe and E.-S. Jang, *J. Ind. Eng. Chem.*, 2021, **96**, 202–212.
38 A. Joe, H.-W. Han, Y.-R. Lim, P. Manivasagan and E.-S. Jang, *Pharmaceutics*, 2024, **16**, 284.
39 D. Pratap, R. Gautam, A. K. Shaw, Vikas and S. Soni, *ACS Appl. Nano Mater.*, 2023, **6**, 21350–21358.
40 L. Vilca-Quispe, J. Alvarado-Gil, P. Quintana and J. Ordonez-Miranda, *Int. J. Thermophys.*, 2010, **31**, 987–997.
41 P. Manivasagan, S. W. Jun, N. T. P. Truong, G. Hoang, S. Mondal, M. S. Moorthy, H. Kim, T. T. V. Phan, V. H. M. Doan and C.-S. Kim, *J. Mater. Chem. B*, 2019, **7**, 3811–3825.
42 S. Bhana, R. O'Connor, J. Johnson, J. D. Ziebarth, L. Henderson and X. Huang, *J. Colloid Interface Sci.*, 2016, **469**, 8–16.
43 R. F. Donnelly, M. J. Garland, D. I. Morrow, K. Migalska, T. R. R. Singh, R. Majithiya and A. D. Woolfson, *J. Controlled Release*, 2010, **147**, 333–341.
44 K. Jiang, D. A. Smith and A. Pinchuk, *J. Phys. Chem. C*, 2013, **117**, 27073–27080.
45 P. Manivasagan, F. Khan, D. R. Dhatchayeny, S. Park, A. Joe, H.-W. Han, S.-H. Seo, T. Thambi, V. G. Phan and Y.-M. Kim, *J. Adv. Res.*, 2023, **48**, 87–104.
46 S. S. Lane, H. B. DuBiner, R. J. Epstein, P. H. Ernest, J. V. Greiner, D. R. Hardten, E. J. Holland, M. A. Lemp, J. E. McDonald and D. I. Silbert, *Cornea*, 2012, **31**, 396–404.
47 E. L. Madsen, M. A. Hobson, H. Shi, T. Varghese and G. R. Frank, *Phys. Med. Biol.*, 2005, **50**, 5597–5618.
48 M. Bauman, G. Gillies, R. Raghavan, M. Brady and C. Pedain, *Nanotechnol*, 2003, **15**, 92–97.
49 G. Lemperle, R. E. Holmes and S. S. M. Lemperle, *Plast. Reconstr. Surg.*, 2001, **108**, 1735–1750.